Multisite bio-stimulating implants magnetoelectrically powered and individually programmed by a single transmitter

Zhanghao Yu, Joshua C. Chen, Yan He, Fatima T. Alrashdan, Benjamin W. Avants, Amanda Singer, Jacob T. Robinson, Kaiyuan Yang

Rice University, Houston, TX

Implantable bioelectronics for electrically modulating activities of specific cells have shown great success and exciting potential in treating a wide range of diseases. Some of the most representative therapies are cardiac pacemakers and neuromodulators for motor function restoration, pain relief and neural disorder treatment [1,2]. While several wireless miniaturized bio-stimulators have been demonstrated [3-6], most of them lack the capability of coordinated multisite stimulation, which is shown to be more effective in many scenarios [1,2]. Equipping an implant with electrode/LED arrays is a straightforward approach to add extra stimulation channels [7-9], but the deployment flexibility of stimulating spots is limited due to leads. [10] shows a wired retinal stimulator array to scale up the driving capability and ensure synchronization, but the heavy use of leads severely limits its applications. A two-site heart pacing system [2] is proposed with two independently powered and controlled implants for flexible leadless deployment. Because the implants are inductively powered by two transmitters (TXs) with frequency multiplexing, they face stricter EM exposure constrains for power transmission, more challenging device synchronization, and limited scalability to more implants. To circumvent these problems, this paper presents a hardware platform for coordinated and miniaturized multisite stimulating implants, wirelessly powered and controlled by a single TX. Magnetoelectric (ME) wireless power transfer with high power and efficiency, low body absorption, and less sensitivity to misalignment [4,5], is co-designed with a robust SoC to enable reliable operation and individual programmability of the implants. The presented system features: (1) robust operation with 2V source amplitude variations, covering up to 40mm distance between TX and implants; (2) individual addressability and programmability of each implant, leveraging PUF IDs; (3) >90% chip efficiency for 1.5-to-3.5V stimulation with fully programmable parameters; (4) no extra TX output power required for additional implants; (5) miniaturized implants with 6.2mm^3 volume and 30mg mass.

The implant integrates a ME film, a capacitor, on-board electrodes, and a SoC. The SoC interfaces with the ME film to receive power and data and drives programmable stimulation. ME induced voltage is rectified to V_{rect} and then converted by an adaptive switched-capacitor power converter (SCPC), which provides proper voltage and buffers energy on the off-chip capacitor for stimulation, and provides V_{DD_H} as a high-voltage supply for SoC. A 1V supply V_{DD_L} is generated by LDO (Fig.1 bottom). Each implant cycles through charging, data transfer and stimulation phases. To maintain reliable synchronized operation of multiple implants under different ME voltages caused by different implantation depth and body movement, the phase transitions are solely controlled by the TX with a short notch of magnetic field (Fig.2 top). Comparator outputs in the active rectifier are reused as watchdog signals to detect the notches. Meanwhile, a global clock is extracted from the source by sensitive clock recovery circuit, ensuring synchronization among all implants.

Individually programing every implant by a shared TX is critical for effective and flexible stimulating therapies. Downlink data transferred by ASK modulation contains a preamble for real-time demodulation threshold calibration, an 8-bit ID for addressing, and a 19-bit data payload for calibration and stimulation settings. The data update controller checks the ID in packet against the on-chip ID to decide whether to accept the new data. The on-chip 8-bit ID is realized with CMOS physical unclonable functions (PUF) leveraging transistor intrinsic variations to cheaply generate and store device-specific IDs (Fig.2 bottom). A inverter chain based PUF design with native NMOS regulation [11] is employed. Because of the narrow operating temperature range and the native voltage regulation, 15-cycle temporal majority voting (TMV) is sufficient to filter out thermal noise and ensure PUF's reliability. The ID generation is triggered by power-on reset signal and clock gated after the ID is loaded to registers.

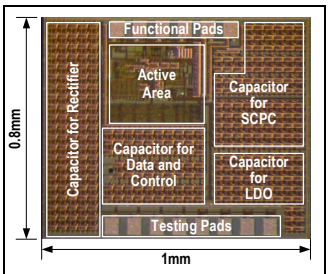

Die micrograph.

Variations of input voltage and power of implants, caused by their distance and misalignment with the TX, are unavoidable in practice, especially for multisite implants. Thus, robust power recovery to support stimulation across a wide source conditions is highly desired. Simply generating a high enough voltage for stimulation driver (V_{DD_stim}) may ensure robustness but will suffer from high power loss and thus heat dissipation [3]. Alternatively, unregulated voltage stimulation by directly driving electrodes with charged capacitors has high efficiency but sacrifices precise charge deposition control [6]. To achieve the desired robustness and efficiency without a complicated feedback and reconfiguration loop as in [12], the proposed SCPC directly generate a V_{DD_stim} that is 10% higher than the desired stimulus amplitude, and relies on the off-chip capacitor and a regulator-style stimulation driver to support regulated mono- and bi-phasic stimulus. Regulation of V_{DD_stim} is realized by disconnecting the capacitor from SCPC, the core of which is a charge pump and a charging controller, once it reaches the desired level. High-speed amplifiers inside the stimulation driver regulates the stimulus. To save power, the amplifier will only be turned on in the stimulation phase. The SCPC also includes an always-on high voltage selector to generate V_{DD_H}, which connects V_{DD_H} to the higher one between V_{rect} and V_{DD_stim} and guarantees cold startup using V_{rect} (Fig. 3).

Fig.4 captures the operation waveforms of the implant. V_{DD_stim} is charged up and regulated to 2.75V, then drops to 2.15V after the 2.5V, 1.2ms bi-phasic stimulation. It is verified that the implant maintains its operation with maximum stimulation amplitude (3.5V) under large ME source variations (1.5–2.7V). 90% stimulating efficiency is achieved as long as the amplitude is larger than 1.5V. Power transfer at various distances are measured, which shows a maximum TX-RX distance of 40mm and a highest power transfer efficiency (PTE) of 1.03%. Individual programming of two implants by a single TX is illustrated in Fig.5 (top left).

An in-vitro test with the a 2cm thick porcine tissue as a medium is conducted (Fig.5, top right), which demonstrates flexible implant deployment covering a space with 35mm radius, and synchronized stimulations by two implants with programmed 0.01-to-0.8ms delays. Based on simulation of the specific absorption rate (SAR) and the electric field induction in a coil-generated 330kHz magnetic field, a magnetic strength of 0.1mT, which is enough to sustain implant's functionality, can be delivered to a depth of 60mm without violating the IEEE C95.1-2019 standards (unrestricted environment).

The proposed system is further validated in-vivo using a transgenic line of Hydra vulgaris as a model for muscle stimulation and a rat model for neural stimulation. Hydra naturally express a calcium sensitive fluorescent protein, GCaMP7b, as well as voltage-gated ion channels. To model synchronous stimulation of muscle tissue, two hydra are used. In order to synchronize the muscle contractions, we provide 3.5V, 20Hz, 1.2ms pulse width, biphasic stimulation pulse trains. This results in >200% GCaMP7b fluorescence increases which demonstrates activation of ion channels resulting in stimulus aligned muscle contractions in both organisms (Fig.6 top left). We also stimulate the sciatic nerve of the rat with varying amplitudes. A graded response in the intensity of the rat leg kick is measured with EMG of the plantar muscles (Fig.6 top right). The comparison table with other bio-stimulating systems is given in Fig. 6 (bottom).

References:

[1] S. Harkema *et al*., Lancet, 2011, DOI: 10.1016/S0140-6736(11)60547-3.
[2] H. Lyu *et al*., Sci. Rep., 2020, DOI: 10.1038/s41598-020-59017-z.
[3] D. K. Piech *et al*., Nat. BME., 2020, DOI: 10.1038/s41551-020-0518-9.
[4] A. Singer *et al*., Neuron, 2020, DOI: 10.1016/j.neuron.2020.05.019.
[5] Z. Yu *et al*., TBioCAS, 2020, DOI: 10.1109/TBCAS.2020.3037862.
[6] H. M. Lee *et al*., JSSC, 2015, DOI: 10.1109/JSSC.2014.2355814.
[7] Y. K. Lo *et al*., ISSCC, 2016, DOI: 10.1109/ISSCC.2016.7418067.
[8] Y. Jia *et al*., ISSCC, 2018, DOI: 10.1109/ISSCC.2018.8310387.
[9] Y. Jia *et al*., ISSCC, 2020, DOI: 10.1109/ISSCC19947.2020.9063065.
[10] T. Tokuda *et al*., TBioCAS, 2010, DOI: 10.1109/TBCAS.2010.2078508.
[11] D. Li *et al*., ISSCC, 2019, DOI: 10.1109/ISSCC.2019.8662537.
[12] H. M. Lee *et al*., JSSC, 2013, DOI: 10.1109/JSSC.2013.2266862.

978-1-7281-7581-2/21/$31.00 ©2021 IEEE

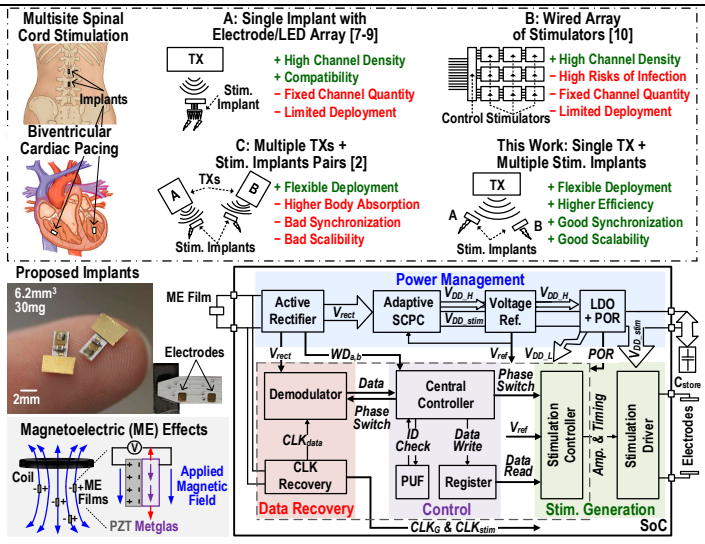

Fig. 1. Concepts of multisite bio-stimulation and various multisite stimulating system structures; illustration of the implant, architecture of its SoC, and principles of ME power transfer for multiple RXs.

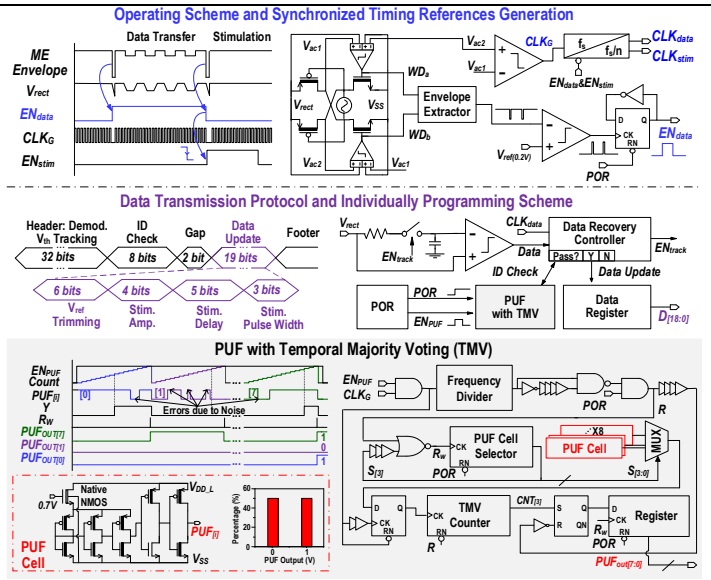

Fig. 2. Diagram of SoC operating phase transition and clock recovery; diagram of data recovery circuitry and schematics of PUF.

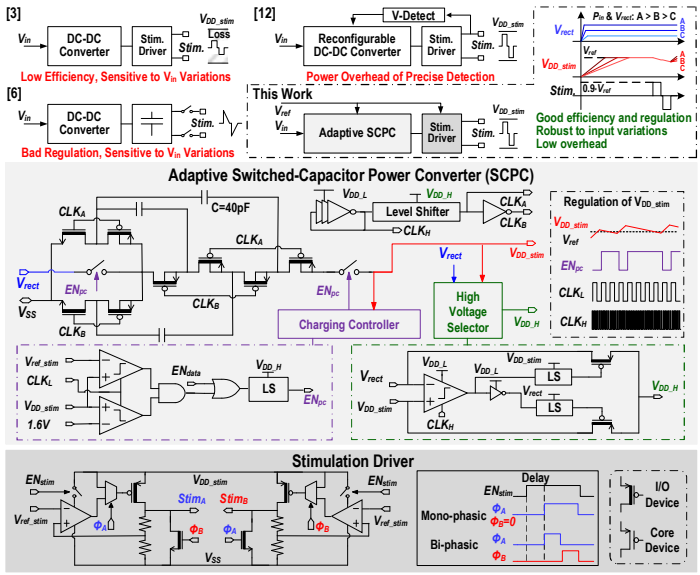

Fig. 3. Principles of the proposed highly efficient voltage stimulation; schematics of adaptive power converter and stimulation driver.

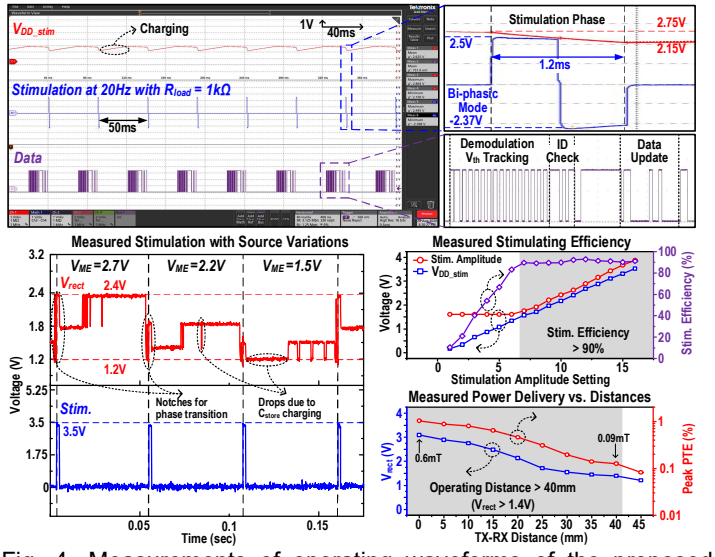

Fig. 4. Measurements of operating waveforms of the proposed implant; 3.5V stimulation with varying ME voltage; stimulating efficiency with various amplitudes; power delivery versus distances.

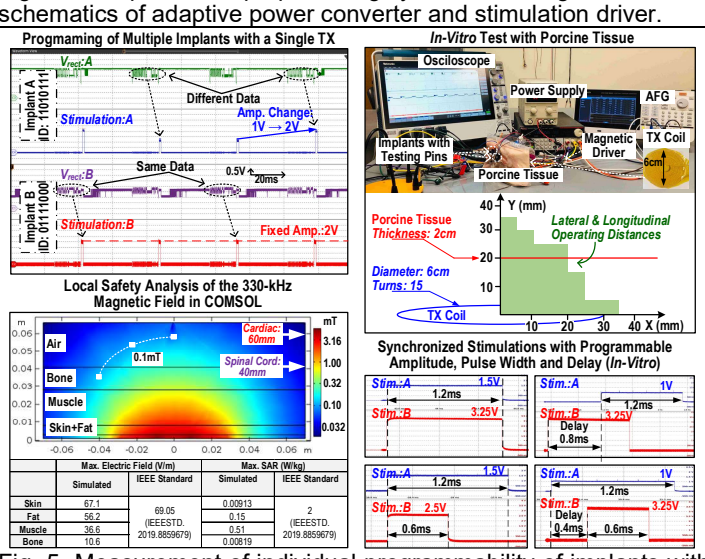

	Max. Electric Field (V/m)		Max. SAR (W/kg)	
	Simulated	IEEE Standard	Simulated	IEEE Standard
Skin	67.1	69.05 (IEEESTD. 2019.8859679)	0.00913	2 (IEEESTD. 2019.8859679)
Fat	56.2		0.15	
Muscle	36.6		0.51	
Bone	10.6		0.00819	

Fig. 5. Measurement of individual programmability of implants with a single TX; safety analysis; in-vitro test with porcine tissue and shmoo plot of operating space; synchronized stimulations and stimulations with programmable delays.

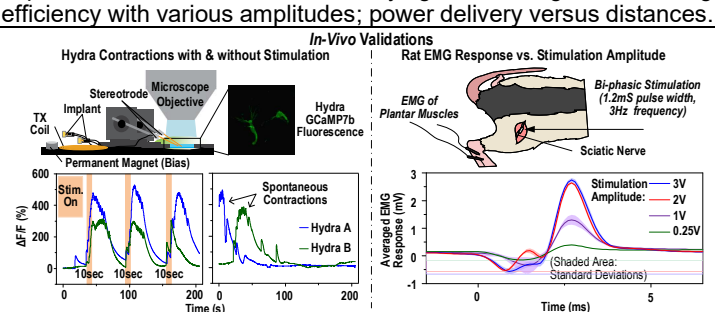

		This Work	ISSCC'16 [7]	ISSCC'18 [8]	Sci. Rep.'20 [2]	ISSCC'20 [9]	Nat. BME.'20 [3]
Target Application		Neural / Cardiac	Neural	Neural	Cardiac	Neural	Neural
Process (nm)		180	180	350	180	350	65
Power Link		Magnetoelectric	Inductive	Inductive	Inductive	Inductive	Ultrasonic
Multisite Stimulation Strategy		Single TX + Multi. Implants	Electrode Array	µLED	Two TXs + Two Implants	Electrode & µLED Array	N/A
Stimulation Mode		Voltage	Current	Optical	Voltage	Optical, Current	Current
Stimulation Parameters (Max., Resolution)	Amplitude	3.5V, 4b	0.5mA, 7b	N/A	3V, Fixed	0.77mA, 5b	0.4mA, 3b
	Pulse Width	1.2ms, 4b	8ms	2ms, 2b	0.3ms, 3 levels	0.64ms, 4b	Continuous
	Frequency	Continuous	Continuous	10Hz, 2b	Continuous	400Hz, 4b	Continuous
Individual Addressability		PUF ID	Multiplexer	Multiplexer	Different $f_{carrier}$	Multiplexer	N/A
SoC Power (W)		9	864	300	3	20700	4
Chip Size (mm²)		1 x 0.8	5.7 x 4.4	1 x 1	0.85 x 0.45	5 x 3	1 x 1
Implant Volume (mm³)		6.2	500	12.2	10.1	N/A	1.7
Max. RX-TX Distance (mm)		40	N/A	7	60	N/A	55

Fig. 6. Synchronous muscle activations of Hydra in response to electrical stimulations; EMG response of rat with various stimulation amplitudes; comparisons with state-of-the-art stimulating systems.